

A STUDY ON THE INFLUENCE OF THE PRIMARY ELECTRON BEAM ON NANODIMENSIONAL LAYERS ANALYSIS

F. MICULESCU*, I. JEPU^a, C. POROSNICU^a, C.P. LUNGU^a,
M. MICULESCU, B. BURHALA

Politehnica University of Bucharest, Faculty of Materials Science and Engineering, Bucharest, 060042, Romania

^aNational Institute for Laser, Plasma and Radiation Physics, Bucharest-Magurele, 077125, Romania

Nowadays scanning electron microscopy (SEM) and energy-dispersive X-ray microanalysis (EDS) are used extensively in nanotechnology and thin films realms. When assessing nanodimensional multilayer systems, by SEM and EDS, new standards of accuracy are required for the analytical data generated by the electron-matter interactions from substrate and the effective thickness of deposited ultrathin films. This study aims to investigate the effect of SEM electron beam energy on the penetration depth on Cu-Ni-Cu-Fe-Ta nanolayered structures of various thicknesses deposited onto Si (100) wafers by thermo-ionic vacuum arc, using extensive microanalytical SEM-EDS measurements and mathematical simulations based on Monte Carlo model. Relationships between the electron beam energy and penetration depth into samples are established. Elemental chemical analyses and films' thickness measurements are performed and the influence of the accelerating voltage of electron beam upon the size and shape of the interaction volume is studied and discussed accordingly.

(Received January 17, 2011; accepted January 24, 2011)

Keywords: nanolayers, SEM, EDS microanalysis, Monte Carlo simulation.

1. Introduction

With the rapid increase of the integration and miniaturization levels in modern industry, the metallic thin films have found many applications in semiconductors industry, microelectronics, spintronics, optical applications, and protective coatings [1]. As methods of investigation, along the transmission electron microscopy (TEM), which provides atomic resolution at this point, scanning electron microscopy (SEM) is one of the most popular tools used for the thin films' characterization. Presently, a great deal of interest is dedicated to the increase of the intrinsic accuracy of analytical data generated from the substrate and the effective thickness of analyzed thin films, and collected by SEM-EDS. Energy-dispersive X-ray microanalysis (EDS) is a technique based on summation and X-ray energy dispersion generated by the accelerated electron bombardment of the samples surface. Depending on the exact choice of beam energy and sample composition a good lateral spatial and in depth resolution can be obtained on a scale ranging from micrometers to nanometers [2-5].

In the field of SEM, the use of precise simulation programs for the electron beam-sample interactions enables the visualization of the interaction volumes between accelerated electron beams and samples, as well as an accurate calculation of the signal intensity resulting from this impact. For this purpose, in the last two decades, the Monte Carlo simulations were used extensively by microscopists. At the beginning, the simulation process was slow and difficult and required a high level of computer skills from users and long computing times. Recently, due to the

continuous advances in the microelectronics industry the high performance computers became almost trivial, which led to the ease of accessibility and the wide use of simulations based on the Monte Carlo model [4,6,7]. Among the advantages of using these analyzing programs lies the possibility of the thoroughly planning and interpretation of the imaging (SEM) and microanalytical (EDS) results. In this regard one of most popular software is CASINO®, which is based on a single scattering algorithm, and models the interaction of low energy beams and thin solid samples. The initial version of the program [6,8] has been developed for experienced users, and presented some limitations regarding the ability to manipulate the data. These issues were addressed in version 2.42, used in this study, by developing a new user interface. The model considers that the electric charge density is uniform throughout the system, and a large scanning area and a defocused beam is assumed in order to have a one-dimensional problem, where the electric field is only a function of the z axis [2]. By microanalytic measurements and mathematical simulations based on Monte Carlo model were established relations between electron beam energy and penetration depth into the samples. A gradually electron trajectory simulation is produced, using random numbers to approximate the scattering angles based on theoretical probability distribution or empirical models. [4–7,9,10]. The depth where X-rays signals is produced during the electron beam-solid matter interaction is strongly dependent on sample density and accelerating voltage. The loss of energy due to inelastic interactions and electron loss or backscattering by elastic interactions are the main factors that determine the size and shape of the interaction volume. The penetration depth of electrons and the sample interaction volume are a function of incidence angle, current, acceleration voltage and atomic number (Z) of the sample [11,12].

The study aims to investigate the effect of electron beam energy on the penetration depth using SEM / EDS analysis of Cu-Ni-Cu-Fe-Ta multilayer structures with different thicknesses deposited by Thermionic Vacuum Arc (TVA) onto Si (100) wafers.

2. Experimental

Cu-Ni-Cu-Fe-Ta type multilayer deposition was obtained using TVA method, at the National Institute of Laser, Plasma and Radiation Physics (INFLPR), Bucharest-Magurele. The principle of this method is a thermoelectronic bombardment from a W filament heated by a current of tens of amperes, to an anode. In the experiments presented in this paper, the voltage applied to the anode, had values of kV order (Table 1). To achieve nanodimensional multilayer films, we used a special anode system, consisting from a cylindrical graphite disc, in which there were positioned four crucibles with the specific deposition materials (Cu, Ni, Fe, Ta). In this way, each material was deposited in the necessary order, without external interference during the deposition session. Through a swinging arm, the deposition material was positioned below the cathode ray gun [13]. The substrates used consisted of Si wafers (100) 12x12 mm, positioned at a distance of 250 mm from the discharger. The deposition rates of each material were determined during the deposition process with a quartz microbalance. The deposition conditions and the thin layers thicknesses are presented in Table 1.

Table 1. Operating parameters and thickness of deposited layers.

Element	U (V)	I (mA)	Rate (Å/s)	Pressure (Torr)	Thickness structure 1 (nm)	Thickness structure 2 (nm)
Cu	600	350	6	2.0×10^{-5}	12	400
Ni	1300	50	0.1	1.1×10^{-5}	5	150
Cu	1800	90	0.2	1.0×10^{-5}	12	400
Fe	2100	120	0.2	9.0×10^{-6}	6	250
Ta	1500	110	0.1	6.5×10^{-6}	3	30
Total					38	1220

After deposition, the samples were placed in the working chamber of the SEM microscope along with standards for the quantitative calibration. Imaging results were obtained with a Philips XL 30 ESEM TMP microscope and X-ray spectra generated were determined and analyzed by an energy dispersive spectrometer EDAX Sapphire, with 128 eV resolution, at University "Politehnica" from Bucharest. Depending on electron beam accelerating voltage and the analyzed elements K, L and M emission lines were used.

Since this study aims to investigate the effect of electron beam energy on the penetration depth the tests were performed at accelerating voltages ranging between 5 and 30 kV in steps of 5 kV for 150 life seconds. The dead time during the spectrum collection was kept below 40%. Samples were positioned at a take off angle (TOA) of 35° from X-radiation detector. During tests, the working conditions were kept in order to minimize any effect on the statistical nature of the production of radiation. Using the program of EDAX analysis, the results were normalized using the ratio of the intensity spectrum. The magnitude of errors should not be significant in this study, as operating conditions were optimized [1, 12].

Conventional energy beam radius is generally defined as $5keV \leq (E_0) \leq 30keV$ (E_0 is the beam energy). When higher energy is applied to electron beam, there are many inelastic collisions and the depth of penetration and lateral spread will be higher. Elastic scattering and the inelastic process of energy loss along the electron beam direction can be described, in simple analytical terms, by Bethe equation and by further expressions developed from it. X-rays are produced through inelastic scattering of electrons. Bethe radius (R) is proportional to beam energy (E_0 in keV), raised to the 1.67 power. According to Kanaya and Okayama's mathematical model, this range can be expressed quantitatively by the relationship:

$$R(\text{nm}) = \frac{27,6AE_0^{1.67}}{(\rho Z^{0.899})} \quad (1)$$

where A is the atomic weight (g/mol), Z is the atomic number and ρ the density (g/cm³). This formula predicts that for the same line of the X-ray radiation, the distance of penetration of electron beam in the sample will be reduced by a factor of 10 when the beam energy is reduced from 20 to 5 keV [1, 13, 14].

The usefulness of a program based on the Monte Carlo model is justified by the possibility of performing a complete simulation for the electrons' paths. For a thorough understanding of the importance of the study, we are briefly describing the stages of work and physical models used by Casino® software to calculate accurately the electrons trajectories according to the present SEM possibilities. To carry out the modelling process we assumed that the electron beam shape is Gaussian. The use of different beam diameters (d) is possible for the microscope used [1, 8, 10, 15]. The actual position of the electron at the impact with the sample is calculated using Eq. (2):

$$X_0 = \frac{d\sqrt{\log(R_1)}}{2\pi}, 0.5 \cdot \cos(2\pi R_2), Y_0 = \frac{d\sqrt{\log(R_1)}}{2\pi}, 0.5 \cdot \cos(2\pi R_3) \quad (2)$$

where R_x are random numbers uniformly distributed between 0 and 1.

The distance between two collisions is evaluated using the equations:

$$L = -\lambda_{ei} \log(R_4) \quad [\text{nm}], \quad (3)$$

$$\frac{1}{\lambda_{ei}} = \rho N_0 \sum_{i=1}^n \frac{C_i \sigma_{ei}^i}{A_i}, \quad (4)$$

where A_i and C_i are atomic weight and mass fraction of element i ; ρ is the volume density (g/cm³), and N_0 is Avogadro's constant.

Total section size [5], σ_i (nm²), for each item in that area is determined using precalculated tabulated values (In this study the effects of inelastic scattering electron deviation were neglected and all the events of electron energy loss were grouped into a continuous function of energy loss) [4, 12]. Using these assumptions, the collisions energy in keV, was calculated using the following equation:

$$E_{i+1} = E_i + \frac{dE}{dS}, \quad (5)$$

$$\frac{dE}{dS} = \frac{-7.85 \cdot 10^{-3} \rho}{E_i} \cdot \sum_{j=1}^n \frac{C_j Z_j}{F_j} \ln \left(1.116 \left(\frac{E_i}{J_j} + k_j \right) \right) \left[\frac{\text{keV}}{\text{nm}} \right], \quad (6)$$

where Z_j and J_j are the atomic number and average ionization potential of element j respectively. k_j is a variable dependent only by Z_j . The elastic collision angle is determined using the precalculated values of the elastic partial interactions and a random number. For areas that contain multiple chemical elements, the responsible atom for the electrons deviation is determined using the overall ratio of the section [6, 8]. These steps were repeated until the electron energy has become less than 50 eV, or until the electrons have left surface of the sample and were detected as backscattered electrons (BE) [4].

As the electron transverse the sample, the program had corrected the trajectories at the interface between two regions crossed. In this case, no angle deviation is calculated and a new random number is generated to calculate the distance L , from the new region. This method produces a more accurate distribution of the maximum penetration depth of electrons in homogeneous and multilayer samples having the same chemical composition as compared with the use of the same random number used to calculate the length L in each new region [4, 12, 16].

The data recording is performed in three-dimensional matrices of cubic elements representing the energy loss of all simulated electrons' trajectories. One of the simulation results was the energy contour lines representation calculated from the centre of the interaction and revealed the percentage of energy that is not included in the line [4]. The lines marked by 10% represent the limit between the area that contains 90% of the absorbed energy and the rest of the sample. Absorbed energy densities are represented by different shades of grey, darker as the density is increasing. From the electron energy loss in the sample we were able to determine the characteristic X-ray radiation generated. X-ray intensities were normalized as a function of depth. The function was calculated from X-ray intensity generated in a ΔZ film thickness with the same chemical composition. This information is useful for a better selection of SEM microscope parameters used in the analytical qualitative and quantitative investigation of nanofilms. The calculations used did not take into account relativistic effects, since these effects become important at energies above 50 keV.

3. Results and discussion

Using the combined signals of secondary electrons (SE) and backscattered electrons (BSE) morpho-compositional images of the two types of samples' surface (Figure 1) were obtained, and some important observations regarding the surface uniformity and ingrowths size were outlined.

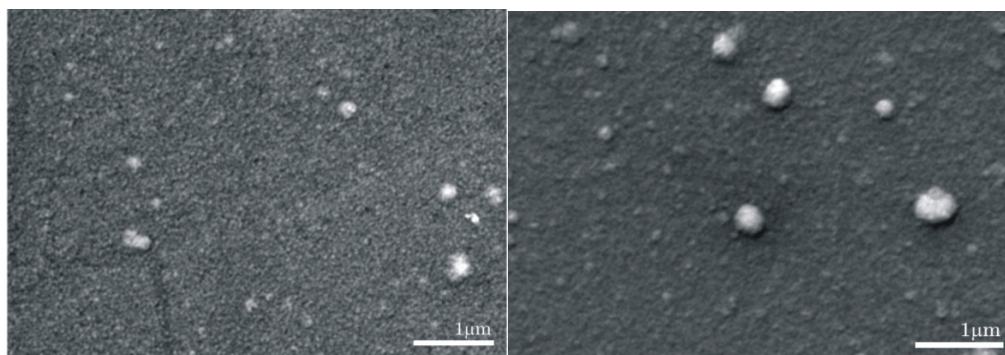


Fig. 1. Top-view SEM surface morphology for the nanodimensional multilayer structures having a total thickness of 38 nm (left) and of 1220 nm (right), respectively.

The sample having layers of total thickness of 38 nm showed a high degree of uniformity, a reduced presence of agglomerates with diameters less than 100 nm being observed. Apart from these topological details, the smooth film's surface is covered with fine grains smaller than 50 nm. The multilayer structure having a total thickness of 1220 nm had a less uniform morphology consisting of larger quasi-equiaxial grains, on its surface being noticed also globular clusters of crystals having dimensions up to 300 nm, well-distributed over the entire sample.

Only the BSE signal has been used to measure the thickness of deposited layers, illustrating different chemical elements in different shades of grey, due to differences of atomic number. These images (Figure 2) allowed the measurement of Cu, Ni and Fe layers' thickness, the thickness of Ta layer being estimated from the deposition parameters. Thus, layers' thickness and sequence, as they were originally calculated, were found for the thin sample as follows: Cu (12 nm), Ni (5 nm), Cu (12 nm), Fe (6 nm) and Ta (3 nm) and for the thick sample: Cu (400 nm), Ni (150 nm), Cu (400 nm), Fe (250 nm) and Ta (20 nm). Due to very small thickness of layers and the limited resolution of W cathode emission source microscopes, in the case of the first sample was not possible to obtain a more detailed image [17].

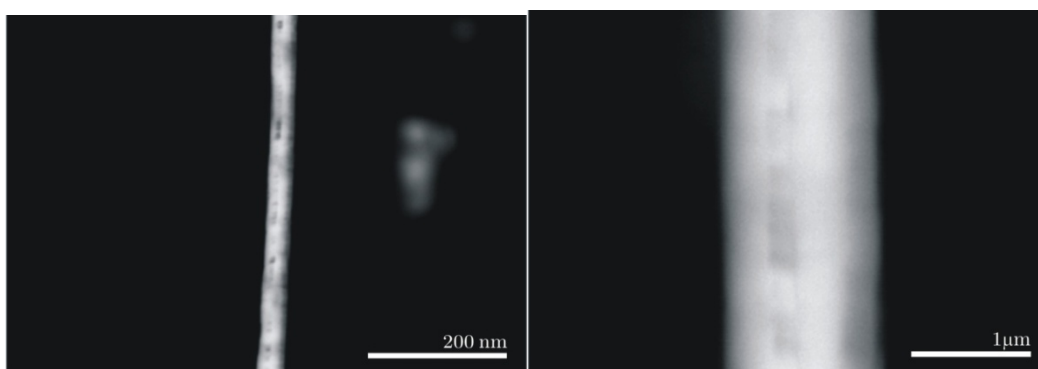


Fig. 2. Backscattered electron cross section images for nanodimensional multilayer structures (left-38 nm, right-1220 nm).

The spectral analysis implied the X-ray emission measurements, which after processing and analysis (Figures 3 & 4) provided the compositional results used to draw the graphs of composition variation function of electron beam acceleration voltage [18–20]. This paper focused only on the spectra obtained with the extreme values and median electrons acceleration voltage of 5, 15 and 30 kV, respectively (Figures 3 & 4).

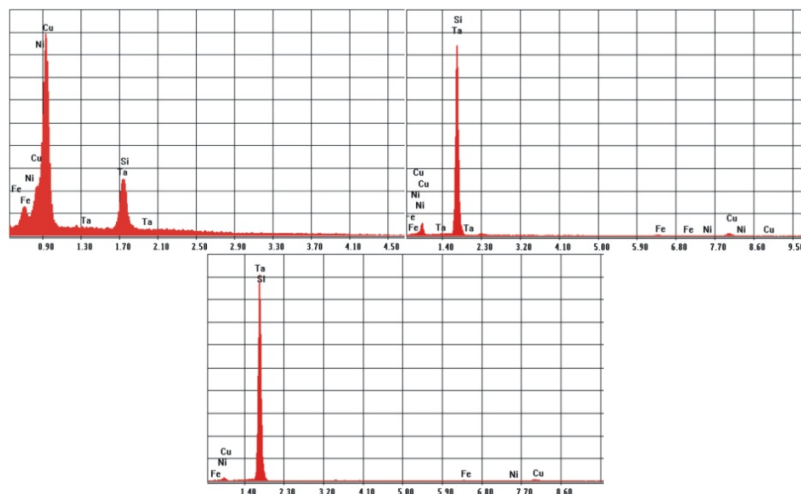


Fig. 3. X-ray emission spectra obtained by investigating samples having a total thickness of 38 nm at 5 kV (left), 15 kV (centre) and 30 kV (right).

The use of high acceleration voltage enabled the excitation of Fe, Ni and Cu K lines, this being impossible at voltages lower than 10 kV. When using the acceleration voltage of 5 kV only L and M excitation lines of the examined elements are observed [21-23]. Due to very small thickness in case of the thinner samples (38 nm), the peaks characteristic to the elements' K lines are very low, and thus the lower energy lines signal summing was also necessary in order to obtain more accurate quantitative results [24].

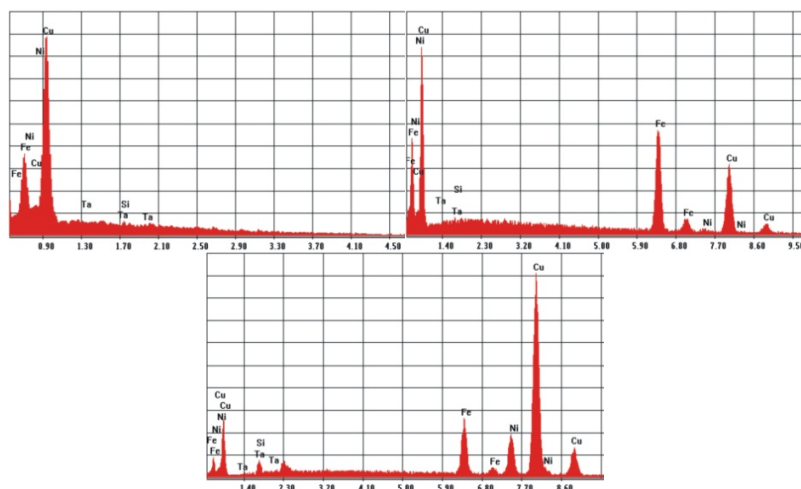


Fig. 4. X-ray emission spectra obtained by investigating samples having a total thickness of 1220 nm at 5 kV (left), 15 kV (centre) and 30 kV (right).

The thicker multilayer structures (1220 nm) offered different characteristic features of X-ray emission compared with thinner samples in the sense that K lines of Cu, Ni and Fe are very pronounced at voltages higher than 10 kV [25]. In order to obtain accurate comparative results, both types of samples were analyzed following the same procedure in a single step.

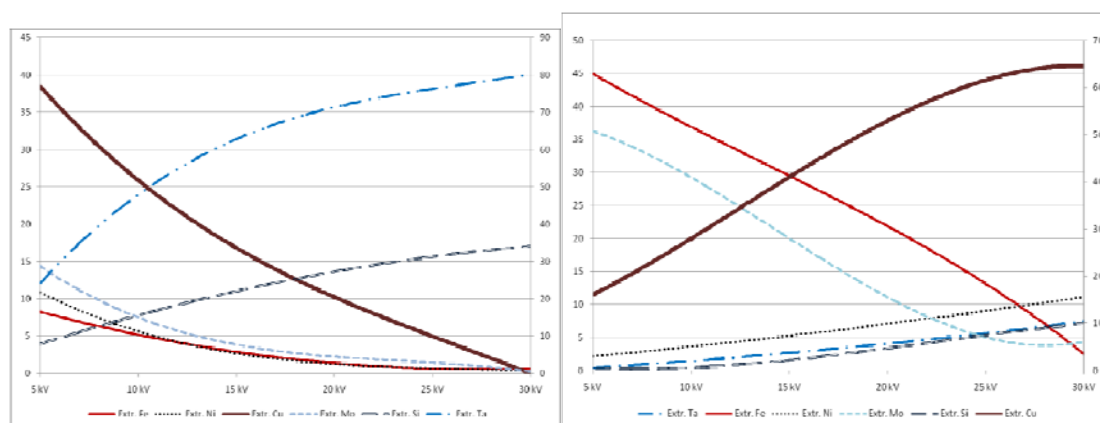


Fig. 5. Variations of elemental concentrations (wt.%) function of electron beam energy (5-30 kV), corresponding to a total thickness of the multilayer structure of 38 nm (left) and 1220 nm (right).

In Figure 5 are graphically represented the concentrational variations (wt. %) of the analyzed chemical elements function of electron beam acceleration voltage, on the secondary axis being represented the Cu distribution. For the thinner structures (38 nm) a gradual increase of Si concentration with electron beam accelerating voltage is observed, increasing from 4% at 5kV to about 35% at 30 kV, while for thicker layers concentration increases from 0% to 15% in the same excitation conditions. A Si concentration of 4% is achieved for the thicker structures at an acceleration voltage of ~20 kV, while a Si concentration of 15% is already exceeded at only 10 kV for the thinner structures. When the thickness of multilayer is greater than 1200 nm, the effect of electron beam energy relative to the atomic percentage of Si shows significant differences due to the metal layers. It can be seen that the variation of Si concentration increases with increasing electron beam energy in both cases. In case of the thinner multilayer structures (38 nm) the dependence is almost linear. Comparing the two graphs, it is confirmed that, even if very different thicknesses of metallic layers were considered, the electron beam energy required to penetrate the layers and to accumulate the same amount of signal increases with film thickness. The electron beam energies required to penetrate the metal layers of different thicknesses are plotted in Monte Carlo modelling representation. Electron beam energy required for penetration displayed a nearly linear relationship with the metallic layer thickness. For the same thickness of different metallic layers, higher electron beam energy is needed when the atomic number of the elements in the deposited layers increases. In addition, with the increase of thickness and atomic number, the detected Si signal, suffers gradual changes from a logarithmic to a linear relationship, function of the electron beam energy.

The corresponding signal of Cu, represented on the graphs on the secondary axis, showed a completely different evolution (dependence). In the case of thinner layers, the concentration drops from 38% at 5 kV to 17% at 15 kV and finally reaches zero at 30 kV. For thicker layers (1220 nm), Cu concentration dramatically increases, from 12% at 5 kV to 30% at 15 kV, and to 62% at 30 kV respectively. A similar concentrational variation, but with lower values, was recorded for Ni. In the case of the thinner layers, Ni presented a descending trend, varying from 12% at 5 kV to 3% at 15 kV, and to 0% at 30 kV respectively. For the thicker metallic layers the increase of Ni concentration is monotonous, being recorded values of 2% at 5 kV, 3% at 15 kV, 10% at 15 kV and of 12% at 30 kV. The Fe concentration showed almost linear decrease for both types of multilayer structures, differing only in the slopes of the two curves, steeper for the thicker structures (dropping from 45% at 5 kV, to 30% at 15 kV, and to 5% at the maximum acceleration voltage), and moderate for the thinner structures (dropping from 8% at 5 kV, to 3% at 15 kV, and to zero at the maximum acceleration voltage). The Ta concentration variation curves showed in both cases increasing trends with acceleration voltage, but the slopes are different. For the thinner structures the Ta concentration increased from 12% at 5 kV to 30% at 15 kV, and finally, to 40% at 30 kV, while in the case of thicker structures the Ta concentration increase from 0% at 5 kV, to 3% at 15 kV, and finally to 7% at 30 kV.

The modelling software allowed the graphically highlighting of the accelerated electron beam interaction volumes with both types of samples. The influence of the chemical elements, the deposited layers' thickness, and of the accelerating voltage of electron beam upon the size and shape of the interaction volume has been studied. In all simulations, 3000 trajectories of electrons in solids were modelled, the electron beam diameter being fixed at 10 nm. Ionization potential was approximated using the Joy and Luo relationship [21] and random numbers were generated using the principles of Press et. al [26]. The dE/dS ratio was calculated as specified by Joy and Luo and effective ionization section was determined using the Casnati relations [23]. It has been noted that when applying a high energy on primary electrons, there are generated more inelastic collisions, which reflect in the increase of penetration depth and lateral spreading [4, 6, 27].

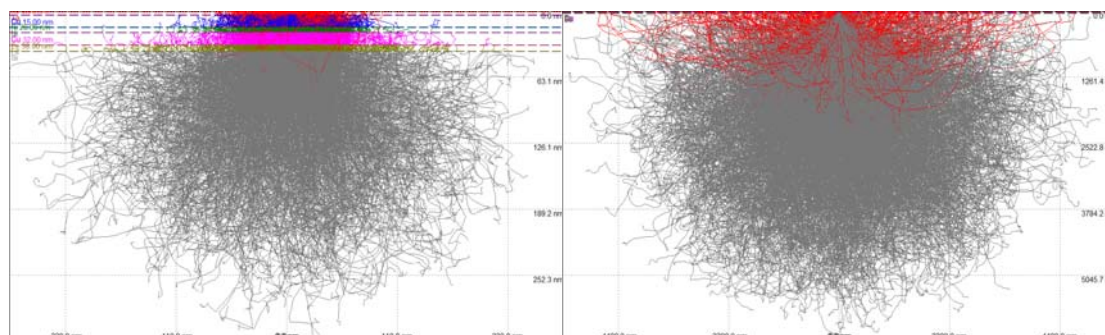


Fig. 6. Interaction volumes modelling for the multilayer samples having a total thickness of 38 nm to 5 kV (left) and 30 kV (right).

Using variable ascending acceleration voltages resulted in interaction volumes with increasing penetration depths. From performed simulations, was observed that in the case of 38 nm layers sample, the main X-ray signal originates even if the lower voltage (5 kV), from the Si substrate. The penetration depth variation is outlined in Figure 10 – left side. In this case, regardless of the chemical element and the thickness of deposited layers (3 to 12 nm), electron acceleration energy was high enough to fully penetrate the multilayer and excite the substrate atoms, which have emitted the preponderant X-ray signal.

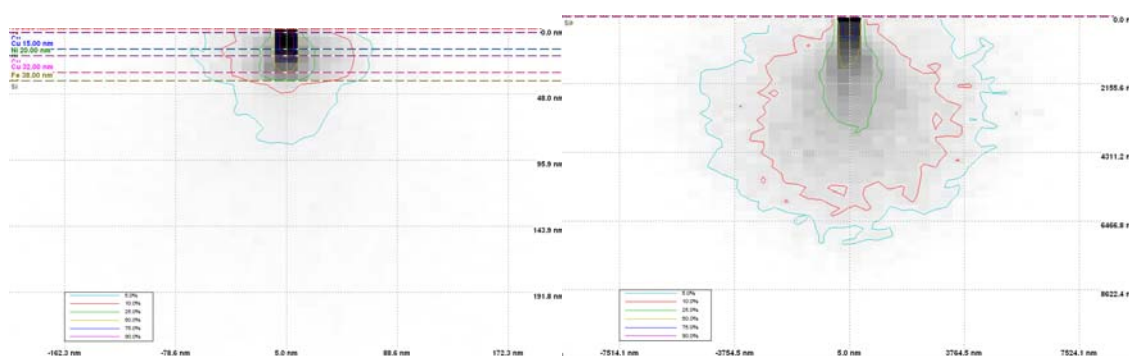


Fig. 7. Energy by Position Distribution corresponding to the multilayer structures having a total thickness of 38 nm at 5 kV (left) and 30 kV (right).

Using *Energy by Position* distribution function [8, 23, 28] variations in the characteristic energy emission levels of different SEM / EDS types of signals have been highlighted. It may be noted that, predominant X-rays signal used in EDS microanalysis comes from the proximity of the characteristic lines of 10% energy contour. This distribution function showed that when low accelerating voltages (5-10 kV) is used, the volume of interaction and consequently the X-ray emission area, covers also the deposited layers, which confirms the achievement of the L and M lines peak emission for small energies.

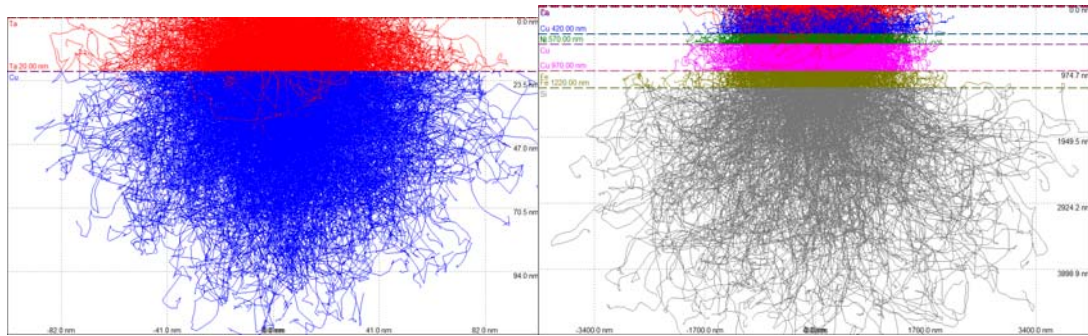


Fig. 8. Interaction volumes modelling for the multilayer structures having a total thickness of 1220 nm at 5 kV (left) and 30 kV (right).

For samples with layers having a total thickness of 1220 nm, the influence of accelerated electron beam on the multilayer structure was more clearly highlighted. When using a low accelerating voltage the excitation is not allowed under deeper layers, but as the electron energy increases, their penetration depth will increase, and X-ray signal output was obtained (Figure 8).

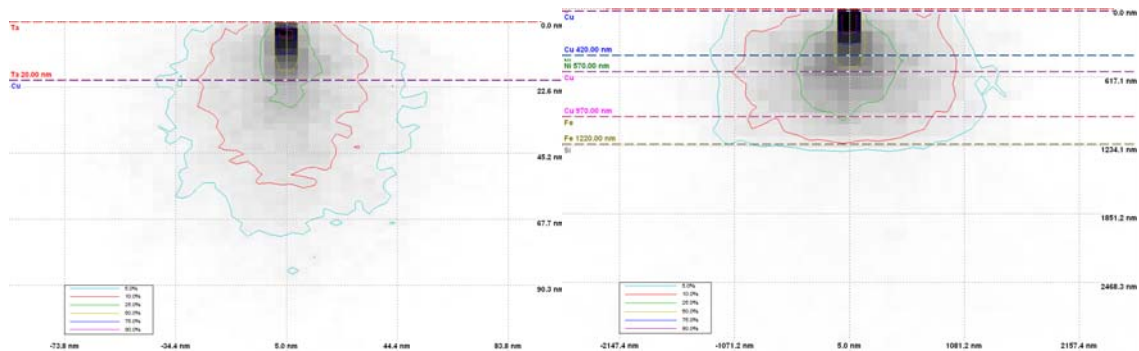


Fig. 9. Energy by Position Distribution corresponding to the multilayer structures having a total thickness of 38 nm (left) and 1220 nm (right).

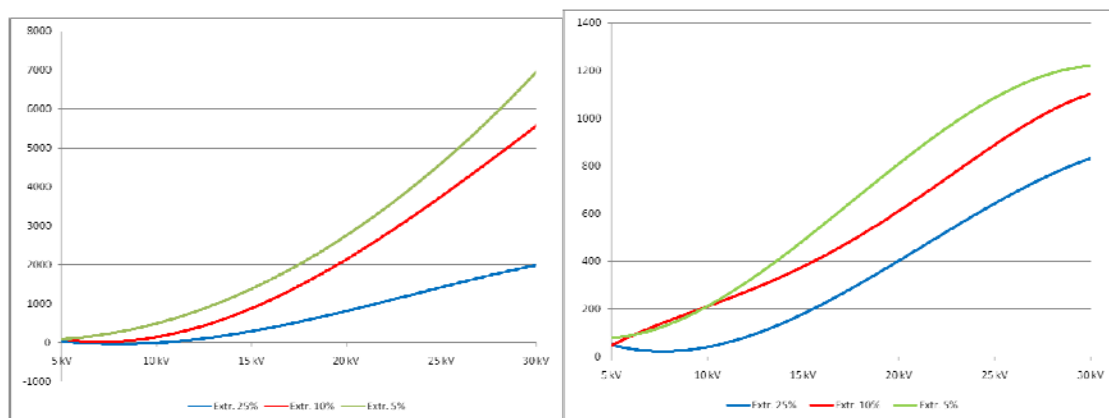


Fig. 10. Energy by Position Distribution function of electron beam energy (5-30 kV), corresponding to the multilayer structures having a total thickness of 38 nm (left) and 1220 nm (right).

From Monte Carlo simulations it can be seen that the layer's atomic number strongly affects the distribution of X-ray radiation generated in the sample. The effects are even more complex when several layers are considered. Based on the above experimental results and simulations, the direct influence of accelerating voltage (electron beam energy) and atomic number on the detected X-ray quantity, was highlighted. When the acceleration voltage is too low, X-rays will not be released because the overvoltage was not reached. As the accelerating voltage increases, both the penetration depth and the size of interaction volume increases, resulting in an

increased detected signal [27, 29-31]. Among other things, the excitation volume defines the area from which X-ray radiation comes. Inelastic scattering probability decreases with the increase of the atomic number Z , so the penetration depth and lateral spreading are lower for heavier elements. In case of a sample with a low atomic number the incident electrons, face low resistance, the volume of interaction becoming oblong of teardrop aspect [32-34]. The energy distribution variation graphs plotted function of position on samples highlighted penetration depths for the studied energies varying between a few nm at 5 kV, to 400 nm at 15 kV, and over 1100 nm at 30 kV, respectively for samples the thicker multilayer structures (total thickness of 1220 nm). In the case of the thinner multilayer structures (total thickness of 38 nm) these penetration depths ranged between 50 nm at 5 kV, 900 nm at 15kV and above 5500 nm at 30 kV.

When an electron flux penetrates into a solid material, electrons can be either elastic or inelastic scattered. Elastic scattering makes the electron beam to deviate from its original direction, resulting in the electrons diffusion through the material. The trajectories of electrons in a material with a high atomic number tend to deviate from their original travel direction more quickly, penetration depth being reduced. In materials with low atomic number, the trajectories deviate slightly from the initial path, and allow deeper penetration. Inelastic scattering progressively reduces the electron beam energy until is captured by solid material, limiting the travel radius of the electron beam inside the solid. For elements with higher atomic numbers, electron capture is easier [26, 33, 35]. The decrease of inelastic scattering with the increase in atomic number leads to a diminution of the penetration depth and the number of collisions.

4. Conclusions

The influence of electron beam accelerating voltage, ranging from 5 to 30 kV, on multilayer structures with total thickness of 38 nm and 1220 nm prepared by TVA, has been studied. The proposed deposition method (TVA) allows the fast deposition of nanolayer structures with some variation of the concentrations of the deposited chemical elements. The SEM images of the deposited films clearly evidenced the presence of some large grains induced during deposition. When nanolayers are analyzed, it is recommended the usage of different acceleration voltages, in order to excite at least the K lines of the low elements and L lines of the heavy elements.

At low energy of the incidence electrons, the absorption effect is less important, because the interaction volume is closer to the surface. If the absorption is taken into account, one can notice the influence of radiation energy to which the phenomenon becomes important. If the X-ray energy is low, absorption is more important for the formation of X-ray radiation intensity. For a higher amount of energy, reduction of ionization is more important. So, dominant phenomena for X-ray energy are reducing ionization or decreasing absorption. If the ionization reduction is the dominant phenomenon, the intensity decreases with the accumulation of electric charge. When the decreasing absorption is predominant the intensity increases with electron beam acceleration voltage increase. These two phenomena are mainly dependent on the incident electron energy and X-ray radiation energy. Changes resulted from X-ray emission intensity can lead to significant errors in obtaining quantitative X-ray microanalysis results for nanosized layers.

The SEM / EDS studies allowed the thickness determination for the Cu, Ni, Fe and Ta layers. At a higher beam energy, the electron beam can penetrate deeper and an intense signal of Si substrate can be detected. The metal layer thickness is in an almost linear relationship with the energy required for electron beam penetration. Based on the experimental results and mathematical models applied in Cu-Ni-Cu-Fe-Ta multilayers study, relations between the detected signal intensity function of the incidence electron beam acceleration voltage were established. If high primary electrons energy is applied, there will be more inelastic collisions, and the penetration depth and lateral spreading will be higher. Inelastic scattering probability decreases with increasing atomic number, thus the penetration depth and spreading are lower for heavier elements. The amount of interaction was simulated and determined using a Monte Carlo model. The simulation results are in good agreement with experimental results. Further systematic experimental studies on different multilayer models are required for a better understanding of the X-ray production and detection phenomena in EDS microanalysis.

Acknowledgements

Authors recognise financial support from the European Social Fund through POSDRU/89/1.5/S/54785 project: “Postdoctoral Program for Advanced Research in the field of nanomaterials”.

References

- [1] F. L. Ng, J. Wei, F. K. Lai, K. L. Goh, *App. Surf. Sci.* **252**, 3972 (2006).
- [2] H. Demers, R. Gauvin, *Microsc. Microanal.* **10**, 776 (2004).
- [3] T. E. Karakasidis, C. A. Charitidis, *Mater. Sci. Eng. C* **27**, 1082 (2007).
- [4] D. Drouin, A. Réal Couture, D. Joly, X. Tastet, V. Aimez, R. Gauvin, *Scanning* **29**, 92 (2007).
- [5] Z. Czyzewski, D. Maccallum, A. Romig, D. Joy, *J. Appl. Phys.* **68**, 3066 (1990).
- [6] P. Hovington, D. Drouin, R. Gauvin, *Scanning* **19**, 1 (1997).
- [7] F. Salvat, J. M. Fernandez-Varea, J. Sempau, X. Llovet, *Radiat. Phys. Chem.* **75**, 1201 (2006).
- [8] T. Eggert, O. Boslau, J. Kemmer, A. Pahlke, F. Wiest, *Nucl. Instrum. Methods Phys. Res. Sect. A-Accel. Spectrom. Dect. Assoc. Equip.* **568**, 1 (2006).
- [9] W. S. M. Werner, *J. Electron. Spectrosc. Relat. Phenom.* **178-179**, 154 (2010).
- [10] B. Gruzza, S. Chelda, C. Robert-Goumet, L. Bideux, G. Monier, *Surf. Sci.* **604**, 217 (2010).
- [11] J. I. Goldstein, D. E. Newbury, D. C. Joy, C. Lyman, P. Echlin, E. Lifshin, L. Sawyer, J. Michael, *Scanning Electron Micro. and X-ray Microanal*, 3rd., Kluwer-Plenum (2002).
- [12] J. L. Pouchou, *Mikrochim. Acta.* **138**, 133 (2002).
- [13] F. Miculescu, C. Lungu, V. Kuncser, N. Miculescu, I. Antoniac, M. Miculescu, *Nanolayers based on giant magnetoresistance effect with multiple applications*, NN10 Conference Proceedings, 106 (2010).
- [14] R. Belkorissata, A. Kadouna, B. Khelifab, C. Mathieu, *Micron* **35**, 543 (2004).
- [15] B. L. Henke, E. M. Gullikson, J. C. Davis, *At. Data Nucl. Data Tables* **54**, 181 (1993).
- [16] K. Kanaya, S. Okayama, *J. Phys. D: Appl. Phys.* **5**, 43 (1972).
- [17] L. Tian, J. Zhu, M. Liu, *Z. An, Nucl. Instrum. Methods Phys. Res. Sect. B-Beam Interact. Mater. Atoms* **267**, 3495 (2009).
- [18] E. D. Boyes, *Mikrochim. Acta* **138**, 225 (2002).
- [19] I. Müllerová, *Scanning Microscopy* **13**, 7 (1999).
- [20] Z. Rouabah, N. Bouarissa, C. Champio, *Appl. Surf. Sci.* **256**, 3448 (2010).
- [21] D. Joy, S. Luo, *Scanning* **11**, 176 (1989).
- [22] D. E. Newbury, *J. Res. NIST* **107**, 605 (2002).
- [23] E. Casnati, A. Tartari, C. Baraldi, *J. Phys. B-At. Mol. Opt. Phys.* **15**, 155 (1982).
- [24] N. de Jonge, N. Poirier-Demers, H. Demers, D. B. Peckys, D. Drouin, *Ultramicroscopy* **110**, 1114 (2010).
- [25] M. Bauer, *J. Magn. Magn. Mater.* **148**, 319 (1995).
- [26] W.H. Press, B.P. Flannery, S.A. Teckolsky, W.T. Vetterling, *Numerical Recipes*, 2nd ed., Cambridge University Press, Cambridge (1992).
- [27] A. Jablonski, *Surf. Sci.* **586**, 115 (2005).
- [28] L. A. Bakaleynikov, E. Yu. Flegontova, E. Zolotoyabko, *J. Electron. Spectrosc. Relat. Phenom.* **151**, 97 (2006).
- [29] H. S. Wong, N. R. Buenfeld, *Cem. Concr. Res.* **36**, 1076 (2006).
- [30] M. Dapor, *Nucl. Instrum. Meth. Phys. Res. Sect. B-Beam Interact. Mater. Atoms* **228**, 337 (2005).
- [31] D. C. Joy, S. Luo, *Scanning* **11**, 176 (1989).
- [32] C. C. Gray, J. N. Chapman, W. A. P. Nicholson, B. W. Robertson, R. P. Ferrier, *X-ray Spectrom.* **12**, 163 (1983).
- [33] O. Jbara, B. Portron, D. Mouze, J. Cazaux, *X-Ray Spectrom.* **26**, 291 (1997).
- [34] P. I. Nikitin, *Sens. Actuator A-Phys.* **106**, 26 (2003).
- [35] J. A. Nielsen, *C. R. Phys.* **9**, 479 (2008).